Journal of Catalysis 272 (2010) 227–234

Contents lists available at ScienceDirect

Journal of Catalysis

journal homepage: www.elsevier.com/locate/jcat

Effect of surface hydroxyls on selective CO_2 hydrogenation over Ni_4/γ-Al_2O_3: A density functional theory study

Yun-xiang Pan [a,b], Chang-jun Liu [a,*], Qingfeng Ge [b,**]

[a] Key Laboratory for Green Chemical Technology of Ministry of Education, School of Chemical Engineering, Tianjin University, Tianjin 300072, China
[b] Department of Chemistry and Biochemistry, Southern Illinois University, Carbondale, IL 62901, USA

ARTICLE INFO

Article history:
Received 31 July 2009
Revised 16 March 2010
Accepted 6 April 2010
Available online 11 May 2010

Keywords:
DFT
Supports
Ni/γ-Al_2O_3
Hydroxylation
CO_2 hydrogenation
Metal–support interaction

ABSTRACT

Catalytic hydrogenation of CO_2 to valuable chemicals or liquid fuels is a promising way to recycle and utilize CO_2. In the present study, elementary steps leading to the formation of formate and CO, two important intermediates in CO_2 hydrogenation on Ni/γ-Al_2O_3, have been explored using the density functional theory (DFT) slab calculations. Two systems: Ni_4 cluster supported on the dry γ-Al_2O_3(1 1 0) surface, D(Ni_4), and on the hydroxylated γ-Al_2O_3(1 1 0) surface, H(Ni_4), have been used to model Ni/γ-Al_2O_3. On D(Ni_4), the reaction energy and activation barrier for formate formation are −0.23 eV and 1.25 eV, respectively, whereas those for CO formation are −0.48 eV and 2.13 eV, respectively. As such, formate formation is preferred kinetically while CO formation is more facile thermodynamically. On H(Ni_4), the reaction energy and activation barrier for formate formation are −0.36 eV and 2.32 eV, respectively, whereas those for CO formation are −0.67 eV and 0.69 eV, respectively. Consequently, CO formation becomes more favorable both kinetically and thermodynamically. These results indicate that hydroxylation of the γ-Al_2O_3 support alters the pathway, and ultimately, the selectivity of CO_2 hydrogenation on Ni/γ-Al_2O_3. This conclusion supports the fact that varying the reaction environment such as water partial pressure is often used to improve the selectivity of a reaction.

1. Introduction

Hydroxylation is a common process that occurs in many processes such as biological conversion and materials processing [1–6]. For oxide-supported metal catalysts, the reaction environment affects the hydroxylation/protonation of the oxide support and modifies the nature of the surface [7–12]. This modification will in turn have an effect on the catalyst-support interaction and further on the reactions taking place on the catalyst [13–18]. For example, Cu(1 1 1) and Cu/TiO_2(1 1 0) are both active toward the water–gas shift (WGS) reaction [13]. However, the apparent activation energy on Cu/TiO_2(1 1 0) is only 8.3 kcal/mol, when compared with 18.3 kcal/mol on Cu(1 1 1). The lower apparent activation energy of Cu/TiO_2(1 1 0) has been attributed to the high activity of TiO_2(1 1 0) toward water dissociation, i.e. hydroxylation of the TiO_2 surface. Lomot and co-worker studied the effect of pretreatment on the activity of a Pd/γ-Al_2O_3 catalyst for the cyclopentane/deuterium exchange reaction [16]. They suggested that an active γ-Al_2O_3-supported catalyst should have two types of sites: Lewis acid sites for cyclopentane binding and surface hydroxyls for proton transfer. The relative concentration of the two types of sites was believed to determine the exchange activity [16]. In the present work, we use a model catalyst, Ni/γ-Al_2O_3, to demonstrate the effect of hydroxylation of the oxide support on the selectivity of the CO_2 hydrogenation.

Climate change resulting from anthropogenic greenhouse gases, mainly CO_2, is considered as a major threat faced by mankind [19]. Recycling CO_2 to useful chemicals or liquid fuel will help to alleviate the greenhouse effect [20–24]. Selective hydrogenation of CO_2 to methanol or methane has been widely explored. Formate and CO are two important intermediates in the selective hydrogenation of CO_2 and have been proposed as precursors to different final products. Formate has been believed to play a crucial role in CO_2 hydrogenation to methanol. For example, Collins et al. [25] considered formate as the precursor for methanol formation in CO_2 hydrogenation on Pd/β-Ga_2O_3. On the other hand, CO is a product of reverse WGS reaction and has been suggested as the key intermediate for methane formation [26–30]. Based on a series of FTIR spectroscopic studies of CO_2 and $CO_2 + H_2$ on the Ru/TiO_2 catalyst, Gupta et al. [30] attributed the linearly adsorbed CO on the Ru^0 sites as a product of either CO_2 reactive adsorption or $CO_2 + H_2$ reaction. The Ru-$(CO)_{ad}$ species reacts with the co-adsorbed or gaseous hydrogen to form methane. These studies indicate that the product of the initial CO_2 hydrogenation steps will determine the distribution of the final products.

* Corresponding author. Fax: +86 22 2789 0078.
** Corresponding author. Fax: +1 618 453 6408.
E-mail addresses: ughg_cjl@yahoo.com (C.-j. Liu), qge@chem.siu.edu (Q. Ge).

0021-9517/$ - see front matter © 2010 Elsevier Inc. All rights reserved.
doi:10.1016/j.jcat.2010.04.003

A number of oxide-supported metal catalysts, including Ni/γ-Al_2O_3, Pd/β-Ga_2O_3 and Cu/ZnO, are active to selectively hydrogenating CO_2 [23–25,31–40]. Among them, the Ni-based catalysts are more suitable for large-scale industrial applications due to the relative low cost and abundance of Ni. Herein, we explored the elementary steps leading to the formation of formate and CO in CO_2 hydrogenation on Ni/γ-Al_2O_3 using the density functional theory (DFT) slab calculations. Two systems: Ni_4 cluster supported on the dry (fully dehydrated) γ-Al_2O_3(1 1 0) surface, D(Ni_4), and on the partially hydroxylated γ-Al_2O_3(1 1 0) surface, H(Ni_4), have been constructed to model Ni/γ-Al_2O_3. The Ni_4 cluster was chosen since it is the smallest unit that provides a three-dimensional structure to probe both metal–metal and metal–support interactions. We adopted the non-spinel γ-Al_2O_3 model [9] and chose the (1 1 0) surface as this surface accounts for more than 80% of the total surface area, and therefore, dominates the surface of γ-Al_2O_3. As demonstrated by Digne et al. [9], the (1 1 0) surface will inevitably be hydrated/hydroxylated under a realistic reaction condition. On the other hand, a direct comparison of CO_2 hydrogenation chemistry over a metal catalyst support on the dry and hydroxylated surfaces will allow us to probe the effect of surface hydroxyls unequivocally. By comparing the potential energy profile of CO_2 hydrogenation on dry support, D(Ni_4), with that on the hydroxylated support, H(Ni_4), we are able to attribute the observed CO_2 hydrogenation selectivity to the existence of surface hydroxyls on the γ-Al_2O_3 surface.

2. Computational methodology and models

All the computations have been performed in the framework of DFT by using the Vienna ab initio simulation package (VASP) [41,42]. The projector augmented wave method [43,44] has been used to describe the nuclei and core electrons. The wavefunctions of valence electrons are expanded on a plane wave basis set with a cut-off energy of 400 eV. The non-local exchange–correlation energy is evaluated using the Perdew–Burke–Ernzerhof functional [45]. A $2 \times 2 \times 1$ *k*-point grid determined by the Monkhorst–Pack method [46] was found to give converged results. Involvement of Ni in the system requires the calculations to include spin-polarization, and our results show that all the structures are of a finite magnetic moment. The atomic structures are relaxed using either the conjugate gradient algorithm or the quasi-Newton scheme as implemented in the VASP code until the forces on unconstrained atoms are <0.03 eV/Å.

The non-spinel γ-Al_2O_3 model [9] has been used to construct surfaces in our previous studies of CO_2 adsorption and activation [8]. In the present study, we use the same size of unit cell to model the γ-Al_2O_3(1 1 0) surface. In all calculations, the bottom two layers are frozen in their bulk positions, whereas the top four layers together with the Ni_4 cluster and the species involved in CO_2 hydrogenation are allowed to relax.

Transition states for the elementary steps leading to the formation of formate and CO are determined in two steps: first, the nudged elastic band method [47] is used to locate the likely transition states; second, the likely transition states are relaxed using a quasi-Newton algorithm until the forces acting on the atoms are <0.03 eV/Å. Frequency analysis has been used to validate the optimized transition state structures.

The combined adsorption energy for co-adsorbed CO_2 and H is defined as:

$$\Delta E_{ad}^{CO_2+H} = -(E_{(CO_2+H)-Ni_4/\gamma\text{-}Al_2O_3} - E_{Ni_4/\gamma\text{-}Al_2O_3} - 1/2E_{H_2} - E_{CO_2})$$

where $E_{Ni_4/\gamma\text{-}Al_2O_3}$ and $E_{(CO_2+H)-Ni_4/\gamma\text{-}Al_2O_3}$ are the total energies of the γ-Al_2O_3(1 1 0) slab with Ni_4 and the slabs simulating CO_2 and H co-adsorbed on Ni_4/γ-Al_2O_3(1 1 0), respectively. E_{CO_2} and E_{H_2} denote the energies of a free CO_2 molecule and a free H_2 molecule, respectively. E_{CO_2} (or E_{H_2}) was computed by placing a single CO_2 molecule (or a single H_2 molecule) in a $10 \times 10 \times 10$ Å^3 cubic box.

3. Results and discussion

A completely dehydrated γ-Al_2O_3 surface is probably best represented by the (1 0 0) surface of the non-spinel γ-Al_2O_3 model [9]. However, our test calculations show that the (1 0 0) surface exposes different surface sites and binds the Ni_4 cluster differently. Therefore, we adopted the completely dehydroxylated γ-Al_2O_3(1 1 0) surface as a reference to examine the effect of surface hydroxylation on the binding of the Ni_4 cluster as well as CO_2 hydrogenation chemistry over the supported catalyst. By keeping similar binding sites for Ni_4 on both dry and partially hydroxylated surfaces, we can focus on the effect of surface hydroxyls on hydrogenation chemistry of CO_2.

3.1. Ni_4 supported on the dry γ-Al_2O_3(1 1 0) surface

The side and top views of the dry γ-Al_2O_3(1 1 0) surface are replotted in Fig. 1a for easy reference. On the surface, the threefold-coordinated aluminum (Al_{3c}), fourfold-coordinated aluminum (Al_{4c}), sixfold-coordinated aluminum (Al_{6c}), twofold-coordinated oxygen ($O_{2c\text{-}1}$, $O_{2c\text{-}2}$ and $O_{2c\text{-}3}$) and threefold-coordinated oxygen ($O_{3c\text{-}1}$, $O_{3c\text{-}2}$ and $O_{3c\text{-}3}$) atoms are exposed, among which Al_{3c}, Al_{4c}, $O_{2c\text{-}1}$, $O_{2c\text{-}2}$ and $O_{2c\text{-}3}$ are coordinately unsaturated. Among three possible structures for a Ni_4 cluster: tetrahedral, rhombic and linear, the tetrahedral structure was shown to be energetically more favorable [48,49]. Consequently, we selected the three-dimensional Ni_4 tetrahedral structure to explore its interaction with the supporting γ-Al_2O_3(1 1 0) surface. Among the sites and structures explored, the structure shown in Fig. 1b, denoted as D(Ni_4), is the most stable. The overall magnetic moment of D(Ni_4) is 4, the same as that of the most stable Ni_4 cluster supported on MgO(0 0 1) [50]. D(Ni_4) is used as the substrate in the

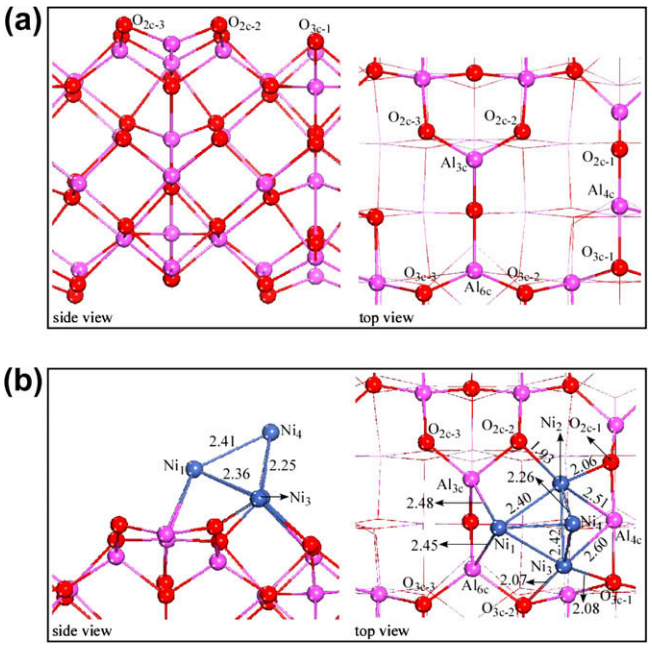

Fig. 1. Structures of (a) the dry γ-Al_2O_3(1 1 0) surface and (b) Ni_4 supported on the dry surface, D(Ni_4). Bond lengths are in Å. Color coding: Red, O atoms; Pink, Al atoms; Blue, Ni atoms. (For interpretation of the references to color in this figure legend, the reader is referred to the web version of this article.)

study of CO_2 adsorption and hydrogenation. The binding energy of the supported Ni_4 cluster in D(Ni_4) with respect to the free tetrahedral Ni_4 cluster is 2.91 eV.

3.2. CO_2 hydrogenation on D(Ni_4)

We determined the adsorption structure of CO_2 and H adatom separately on D(Ni_4) and provided the results in the supporting information. We then explored the co-adsorption of CO_2 and H on D(Ni_4). The most stable configuration for the co-adsorption of CO_2 and H on D(Ni_4), D-1, is shown in Fig. 2. The combined adsorption energy for the co-adsorbed CO_2 and H is 1.46 eV. D-1 serves as the starting configuration for CO_2 hydrogenation to formate in Section 3.2.1 and to CO in Section 3.2.2. For clarity, the intermediates, transition states and products involved in CO_2 hydrogenation on D(Ni_4) are prefixed with D. The oxygen atoms of CO_2 will be distinguished as O_a and O_b if the two atoms are in inequivalent positions.

3.2.1. CO_2 hydrogenation to formate on D(Ni_4)

The potential energy profile following the pathway from D-1 to D(formate) is presented in Fig. 3 as a black line. The structures of all the intermediates, transition states and product involved in the process are shown together with the potential energy profile.

The formation of D(formate) begins with the formation of an intermediate, D(IM1), through a transition state, D(TS1). The conversion from D-1 to D(IM1) is endothermic, by 0.30 eV, with a significant activation barrier (1.02 eV). This step breaks the C–Ni_1, O_a–Ni_1 and O_b–Ni_4 bonds and forms an O_a–Ni_4 bond. In D(IM1), the O_aCO_b species binds the substrate through a C–Ni_4 bond (1.94 Å) and the newly formed O_a–Ni_4 bond (1.91 Å). The second step converts D(IM1) into another intermediate, D(IM2). This step corresponds to the migration of the H adatom from a threefold site in D(IM1) to a twofold site in D(IM2), as shown in Fig. 3. The second step is endothermic, by 0.12 eV, without an apparent barrier. This is consistent with the H diffusion potential energy surface on Ni(1 1 1) where the bridge site is a flat-top maximum [51]. In the third step, the H adatom is transferred from the Ni site to the C atom through transition state D(TS2), forming a C–H bond in intermediate D(IM3). This step is exothermic, by 0.17 eV, with a relatively high activation barrier (0.83 eV). D(IM3) is an unidentately bound formate species. In the last step, the unidentately bound formate species relaxes into a more stable and bidentately bound formate species. The last step is exothermic, by 0.48 eV, with a small activation barrier of 0.10 eV.

In D(formate), the formate (O_aCHO_b) species binds the substrate through the O_a–Ni_4 (1.89 Å) and O_b–Ni_1 (1.95 Å) bonds, as shown in Fig. 3. The C–O_a and C–O_b bonds are 1.28 Å and 1.27 Å, respectively, and the O_a–C–O_b angle is 127°. These structural properties are similar to those observed in formate adsorption on the Ni surfaces [52–56].

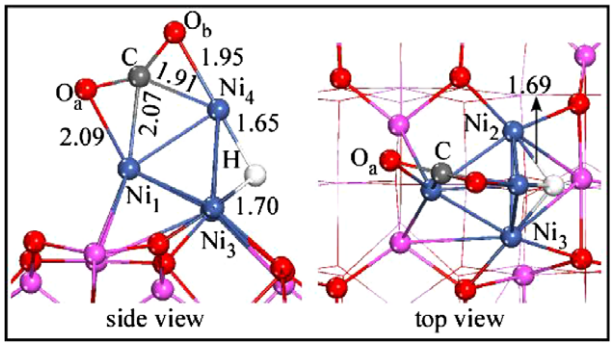

Fig. 2. Structure of the co-adsorbed CO_2 and H on D(Ni_4). Bond lengths are in Å. Color coding: White, H; Gray, C; others are the same as in Fig. 1. (For interpretation of the references to color in this figure legend, the reader is referred to the web version of this article.)

3.2.2. CO_2 hydrogenation to CO on D(Ni_4)

The pathway for CO formation also starts from D-1. The product of this process is co-adsorbed CO and OH, denoted as D(CO + OH). The potential energy profile from D-1 to D(CO + OH) is shown in Fig. 3 as a red line. The structures of the intermediates, transition states and product involved in the process are presented along with the potential energy profile.

This pathway starts from the activation of the H adatom from the threefold site in D-1 to the twofold site in D(IM4). Similar to the second step in the formate pathway, this step is slightly endothermic, by 0.18 eV. In the second step, H migrates from binding Ni_3 and Ni_4 in D(IM4) to binding the O_b atom of the CO_2 fragment in D(IM5), leading to a *trans*-carboxyl (*trans*-COOH) species in D(IM5) through the transition state D(TS4). The second step is endothermic, by 0.53 eV, with a significantly high activation barrier (1.95 eV). The third step corresponds to isomerization from the *trans*-COOH species in D(IM5) to the *cis*-COOH species in D(IM6) through transition state D(TS5). The third step is exothermic, by 0.11 eV, and has an activation barrier of 0.36 eV. In the last step, the *cis*-COOH species in D(IM6) dissociates into co-adsorbed CO and OH groups in D(CO + OH) through transition state D(TS6). In D(CO + OH), the OH group binds the substrate through a newly formed O_b–Ni_4 bond (1.75 Å) while CO interacts with the substrate through a C–Ni_1 (1.71 Å) bond. The reaction energy and the activation barrier for the last step are −1.08 eV and 0.64 eV, respectively.

3.3. Ni_4 supported on the hydroxylated γ-Al_2O_3(1 1 0) surface

Before presenting the results of how hydroxylation of the γ-Al_2O_3(1 1 0) surface affects CO_2 hydrogenation, we first examine how surface hydroxylation modifies the interaction between the Ni_4 cluster and the surface. We use the hydroxylated γ-Al_2O_3(1 1 0) surface established in our previous work [8] as the support for the Ni_4 cluster. The schematic views of the surface are redrawn in Fig. 4a as a reference. The key feature of the surface is that a hydroxyl group (O_wH_a) binds to a surface Al_{3c} site, whereas a proton (H_b) binds to a surface $O_{2c\text{-}3}$ site, forming two surface OH groups in one unit cell.

A number of sites on the above hydroxylated surface have been explored for Ni_4 adsorption. The most stable adsorption configuration, denoted as H(Ni_4), is shown in Fig. 4b. In H(Ni_4), the Ni_4 cluster interacts with the surface through three Ni atoms (Ni_1, Ni_2 and Ni_3). This overall magnetic moment of H(Ni_4) is 2, indicating quenching of spins in the presence of surface hydroxyls. The binding energy of the Ni_4 cluster in H(Ni_4) is 1.87 eV, which is 1.04 eV lower than that in D(Ni_4). The decreased binding energy indicates that the presence of the hydroxyls on the surface weakens the binding of Ni_4 on the surface. On the other hand, hydroxylation of the surface at this OH coverage leads to an energy gain of 2.36 eV with respect to a dry surface and gas phase H_2O [8]. Therefore, H(Ni_4) was selected as the substrate in the following study for CO_2 hydrogenation.

3.4. CO_2 hydrogenation on H(Ni_4)

In order to map out the CO_2 hydrogenation pathways, we need to establish the co-adsorption configuration of CO_2 and H on H(Ni_4). Among structures examined, H-1 shown in Fig. 5 is the most stable configuration for the co-adsorption of CO_2 and H on H(Ni_4). The combined adsorption energy for the co-adsorbed CO_2 and H_c is 2.52 eV. We also examined the adsorption of CO_2 and H on H(Ni_4) individually and provided the results in supporting infor-

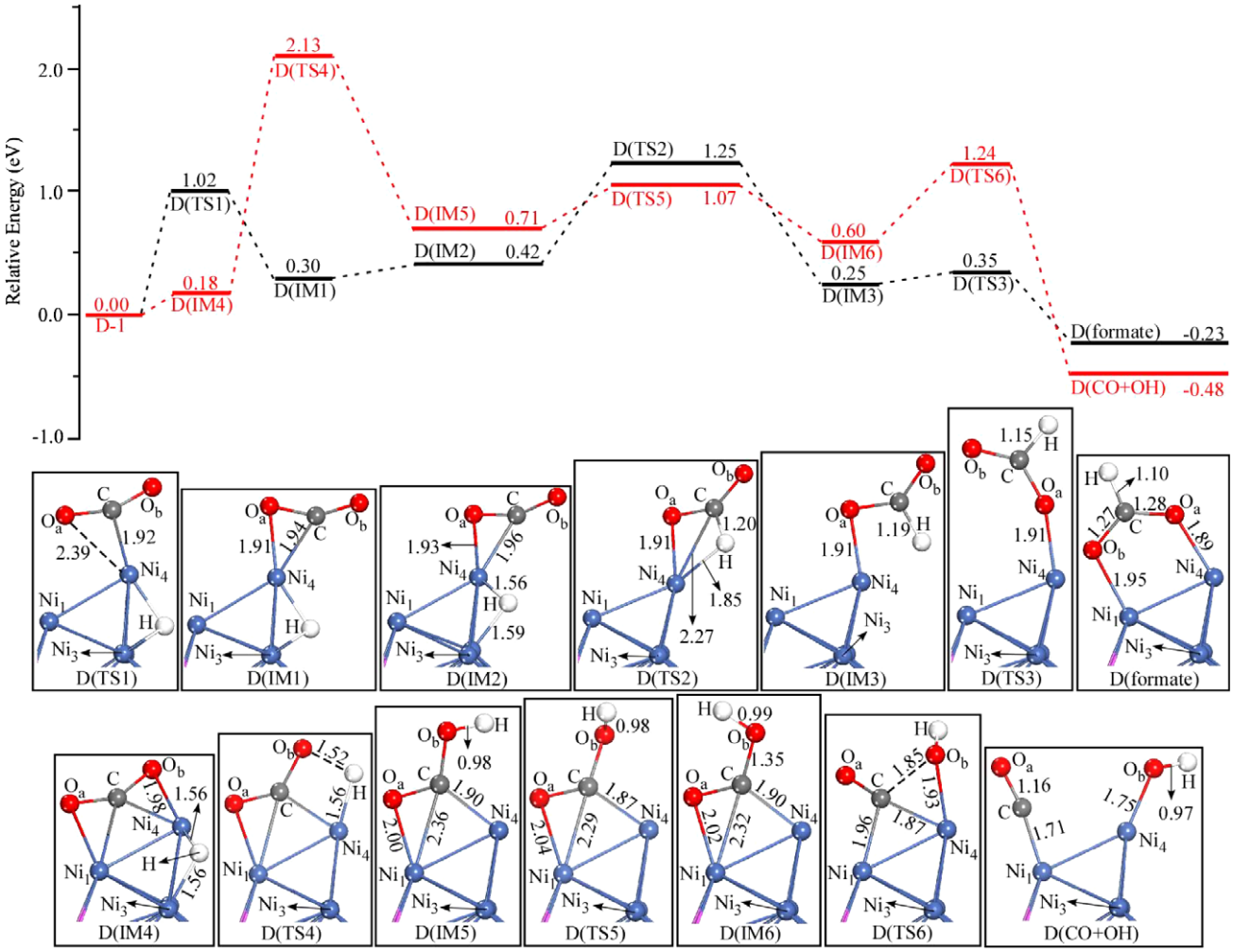

Fig. 3. Potential energy profiles for CO_2 hydrogenation to formate (black line) and to CO (red line) on D(Ni_4). Structures of the intermediates, transition states and products are also shown. Bond lengths are in Å. See Figs. 1 and 2 for color coding. (For interpretation of the references to color in this figure legend, the reader is referred to the web version of this article.)

mation. In the following presentation, we use H_c to distinguish the H adatom from those resulting from dissociative adsorption of H_2O (H_a and H_b). The names of all the intermediates, transition states and products formed on H(Ni_4) are prefixed with H to distinguish them from those on the fully dehydrated surface.

3.4.1. CO_2 hydrogenation to formate on H(Ni_4)

Using H-1 as the starting configuration, we studied formate formation from co-adsorbed CO_2 and H_c. The potential energy profile from H-1 to H(formate) is shown in Fig. 6 using a black line. Three intermediates, H(IM1), H(IM2) and H(IM3), are involved in the process. These intermediates partition the process into four steps: (i) breaking the C–Ni_1 bond through transition state H(TS1); (ii) breaking the C–Ni_4 bond through transition state H(TS2); (iii) binding the O_a atom to the Ni_1 atom; and (iv) transfer of the H_a atom from the O_a atom to the carbon atom through transition state H(TS3). The structures of H(IM1), H(IM2), H(IM3), H(TS1), H(TS2), H(TS3) and H(formate) are shown on the potential energy diagram.

In the first step, the carbon atom breaks from the Ni_1 atom through transition state H(TS1), leading to the formation of H(IM1). In H(IM1), the *trans*-COOH species interacts with the substrate through the C–Ni_4 (1.84 Å) and O_b–Ni_4 (2.22 Å) bonds. The first step is endothermic, by 0.70 eV, and has an activation barrier of 0.79 eV. In the second step, the C–Ni_4 bond breaks through transition state H(TS2). In H(IM2), the *trans*-COOH species adsorbs on the substrate through the O_b–Ni_4 bond (1.84 Å). The reaction energy and the activation barrier of the second step are 0.84 eV and 0.90 eV, respectively. The third step converts H(IM2) to H(IM3), making the O_a atom of the *trans*-COOH species bind the Ni_1 atom. The third step is slightly exothermic, by only 0.07 eV. The last step converts H(IM3) to H(formate) by transferring the H_a atom from the O_a atom to the carbon atom through transition state H(TS3). The last step is strongly exothermic, by 1.83 eV, and has an activation barrier of 0.85 eV.

As shown in Fig. 6, the formate (O_aCHO_b) adsorbs across the Ni_1–Ni_4 bridge site in H(formate). The O_a atom binds the Ni_1 atom with a distance of 2.00 Å, and the O_b atom points to the Ni_4 atom with a distance of 1.88 Å. The distances of the C–O_a and C–O_b bonds are 1.27 Å and 1.28 Å, respectively, and the O_a–C–O_b angle is 126°.

3.4.2. CO_2 hydrogenation to CO on H(Ni_4)

H-1 is also the starting configuration for CO_2 hydrogenation to CO on H(Ni_4). We explored three possible pathways for CO_2 hydrogenation to CO on H(Ni_4) and only discuss the most favorable route as shown in a red line in Fig. 6. The details of the other two less favorable pathways will be presented in supporting information. Again, we provide the structures of all the intermediates, transition states and products involved along the potential energy profile.

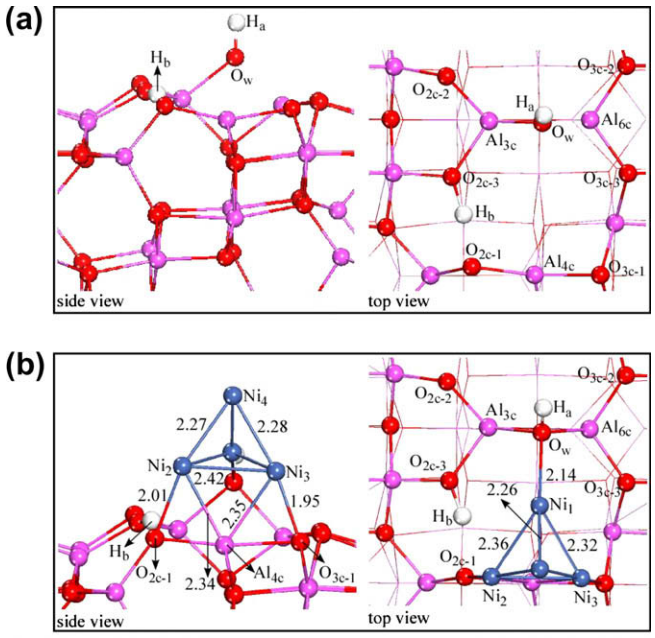

Fig. 4. Structures of (a) the hydroxylated γ-Al_2O_3(1 1 0) surface and (b) Ni_4 supported on the hydroxylated γ-Al_2O_3(1 1 0) surface, H(Ni_4). Bond lengths are in Å. See Figs. 1 and 2 for color coding. (For interpretation of the references to color in this figure legend, the reader is referred to the web version of this article.)

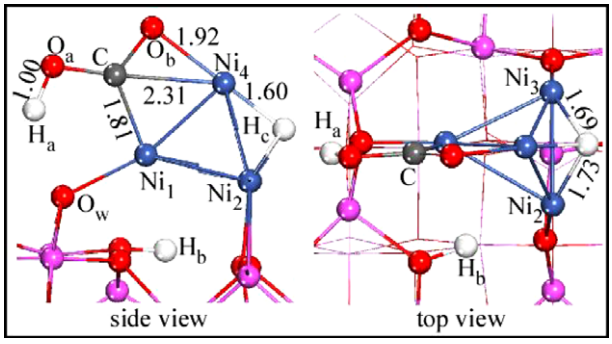

Fig. 5. Structure of the co-adsorbed CO_2 and H on H(Ni_4). Bond lengths in Å. See Figs. 1 and 2 for color coding. (For interpretation of the references to color in this figure legend, the reader is referred to the web version of this article.)

CO_2 hydrogenation to CO on H(Ni_4) begins with isomerization of H-1 to H(IM4) through transition state H(TS4). This step transfers the H_a atom from beneath the O_a atom to above the O_a atom, converting *trans*-COOH to *cis*-COOH. This step is endothermic by 0.17 eV and has an activation barrier of 0.42 eV. The *cis*-COOH species in H(IM4) can be dissociated into CO and OH, producing $H(CO + OH)_1$, as shown in Fig. 6. The conversion from H(IM4) to $H(CO + OH)_1$ involves an intermediate, H(IM5). In H(IM4), the H_a and O_a atoms are in the plane formed by the O_b, Ni_1 and Ni_4 atoms, but, in H(IM5), the H_a and O_a atoms are out of the plane with the O_a atom approaching the Ni_2 atom. The subsequent conversion from H(IM5) to $H(CO + OH)_1$ proceeds through transition state H(TS5). The reaction energy and activation barrier for the conversion from H(IM4) to $H(CO + OH)_1$ are −0.11 eV and 0.52 eV, respectively. The O_aH_a group in $H(CO + OH)_1$ can combine with the proton (H_b) on the hydroxylated γ-Al_2O_3(1 1 0) surface to form an adsorbed water molecule. The process from $H(CO + OH)_1$ to $H(CO + H_2O)_1$ describes the combination process. In this combination, the proton (H_b) migrates from the surface $O_{2c\text{-}3}$ atom to the O_a atom of the O_aH_a group through transition state H(TS6), producing an adsorbed H_2O molecule in $H(CO + H_2O)_1$. In $H(CO + H_2O)_1$, the H_2O molecule interacts with the substrate through the O_a–Ni_2 bond (2.00 Å). As shown in Fig. 6, this combination is exothermic, by 0.73 eV, with an activation barrier of 0.50 eV.

3.5. General discussion

Fig. 7a shows a simplified potential energy diagram by only including the highest barrier for conversion of CO_2 to formate and CO on D(Ni_4). As shown in the figure, on D(Ni_4), the reaction energy and activation barrier, with respect to the co-adsorbed CO_2 and H, for formate formation are −0.23 eV and 1.25 eV, respectively, whereas those for CO formation are −0.48 eV and 2.13 eV, respectively. Consequently, formate formation is favorable kinetically, whereas CO formation is preferred thermodynamically. Transferring the H adatom from the supported Ni_4 cluster to the adsorbed CO_2 is an essential step in CO_2 hydrogenation. We performed Bader charge analyses for all the intermediates and transition states involved in H transfer on D(Ni_4) in order to determine the charge transfer accompanying each reaction step. Along the route for formate formation, the electronic charge on H changes from −0.05 |*e*| in D(IM2) to +0.11 |*e*| in D(TS2), and then to +0.12 |*e*| in D(IM3). On the other hand, following the pathway for CO formation, the electronic charge on H varies from -0.05 |*e*| to +0.16 |*e*|, and then to +0.59 |*e*|. Clearly, the variation of the electronic charge on H in CO formation is much more pronounced than that in formate formation. This is consistent with the fact that the H atom becomes more proton-like in the product state of the CO formation pathway and may be responsible for the high activation barrier.

A summary potential energy diagram for CO_2 hydrogenation to formate and CO on H(Ni_4) is shown in Fig. 7b. On H(Ni_4), the reaction energy and activation barrier, with respect to the co-adsorbed CO_2 and H, for formate formation are −0.36 eV and 2.32 eV, respectively, while those for CO formation are −0.67 eV and 0.69 eV, respectively. Therefore, CO formation becomes more favorable both kinetically and thermodynamically on H(Ni_4). We also performed Bader charge analyses for the intermediates and transition states involved in H transfer on H(Ni_4). On H(Ni_4), the H atom transferred is the H_a atom of the O_wH_a group on the hydroxylated γ-Al_2O_3(1 1 0) surface. Transferring H_a from O_w to O_a leads to the formation of a carboxyl species. The electronic charge on H_a only increases by 0.04 |*e*| accompanying this transfer. Dissociation of the carboxyl species leads to CO formation. On the other hand, in order to form formate, H_a has to be transferred from O_a to the carbon atom, converting H(IM3) to H(formate) through transition state H(TS3). From H(IM3) to H(TS3), and then to H(formate), the electronic charge on H_a changes from +0.57 |*e*| to +0.42 |*e*|, and then to +0.22 |*e*|. The charge separation associated with formate formation on the hydroxylated surface contributes to the high activation barrier.

Our results show that the dominant product of the initial steps of CO_2 hydrogenation on D(Ni_4) is formate, whereas CO is mainly produced on H(Ni_4). Since formate is the key intermediate in CO_2 hydrogenation to methanol, whereas CO is the product of a reverse WGS reaction and likely leads to methane [26–29,57,58], the product from these initial steps is expected to affect the distribution of the final products. These results demonstrate that hydroxylation of the oxide support plays an important role in determining the selectivity of CO_2 hydrogenation on oxide-supported metal catalysts. The concept can be applied to analyze previous experimental results and help to select new catalyst materials. Oxides such as ZnO are known to have a low affinity toward water and, therefore, are difficult to be hydroxylated [59]. This may be the reason that ZnO has been used as a key ingredient in methanol synthesis catalysts. On the other hand, oxides such as γ-Al_2O_3 and TiO_2 have a greater affinity toward water [9,13], and the presence of hydroxyls

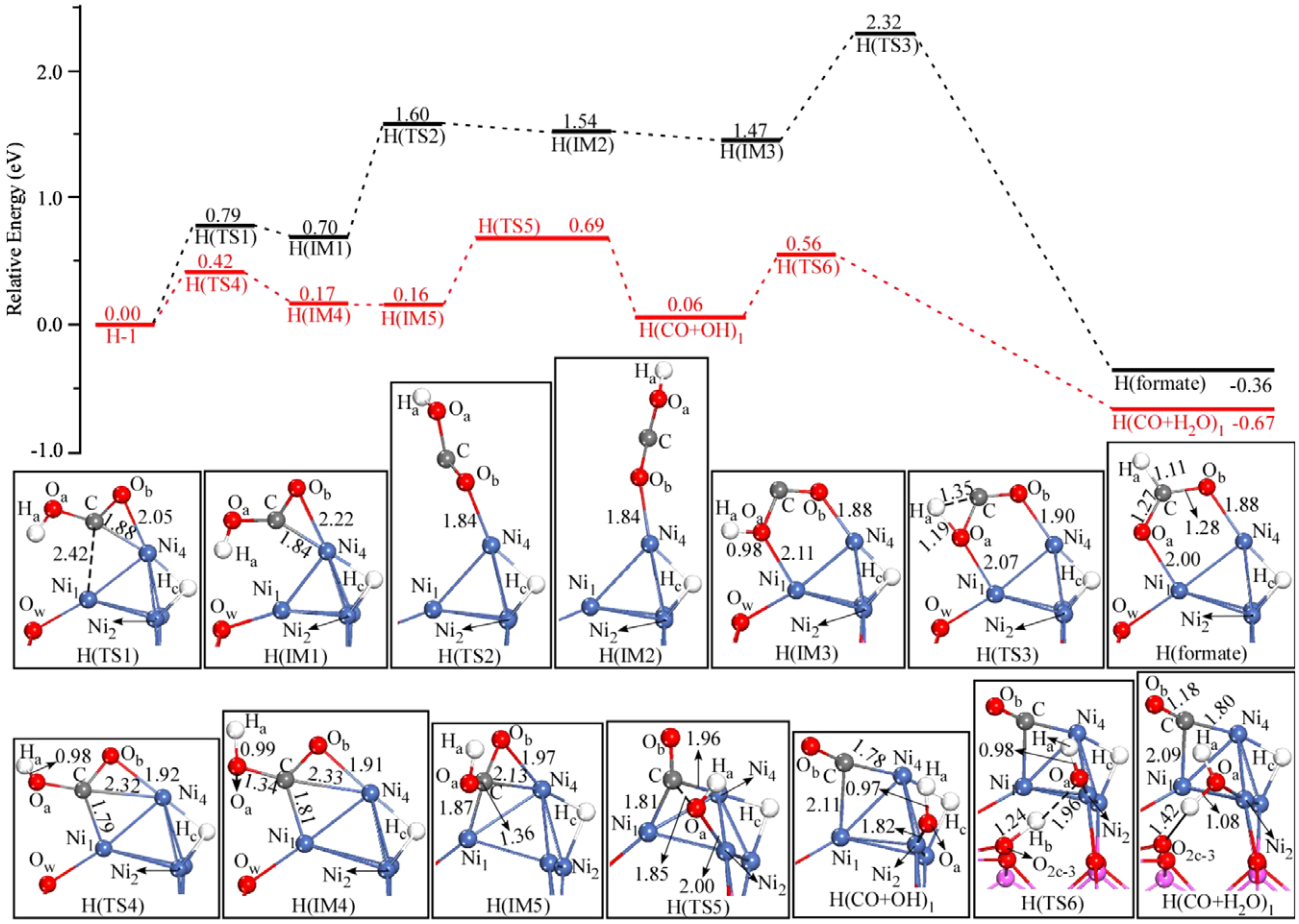

Fig. 6. Potential energy diagrams for CO_2 hydrogenation to formate (black line) and to CO (red line) on H(Ni_4). Structures of the intermediates, transition states and products are also shown. Bond lengths are in Å. See Figs. 1 and 2 for color coding. (For interpretation of the references to color in this figure legend, the reader is referred to the web version of this article.)

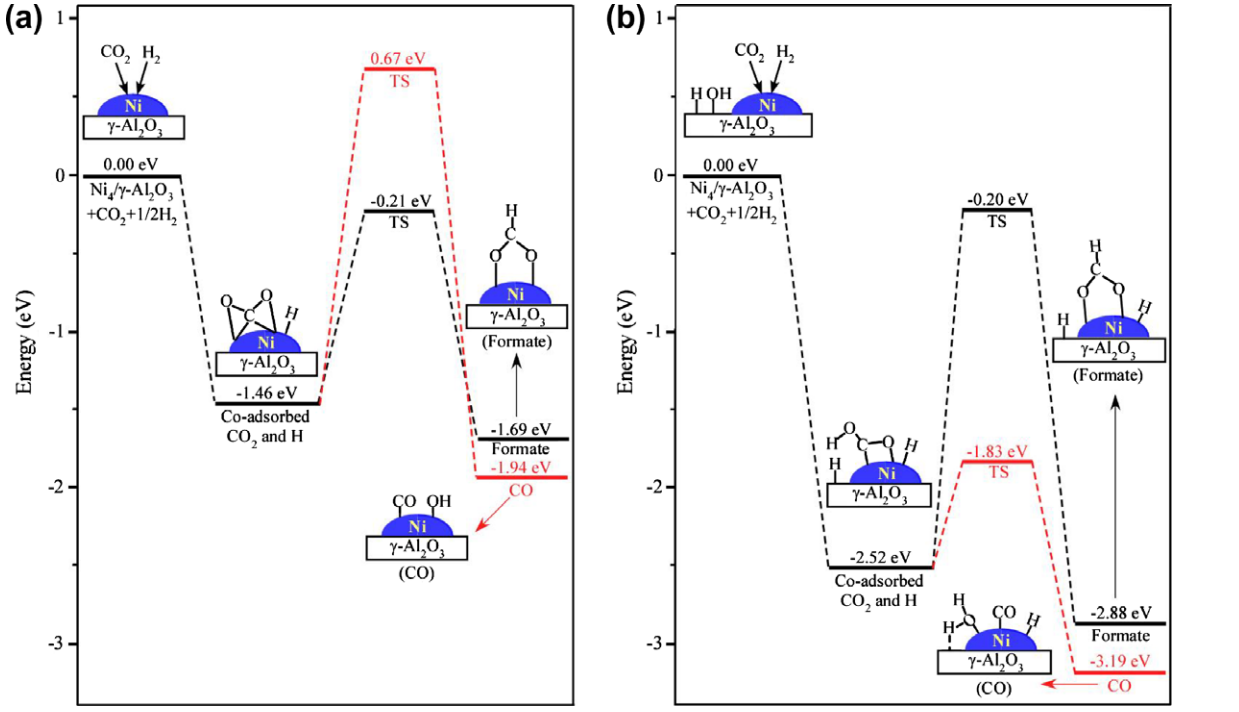

Fig. 7. Schematic potential energy diagrams of CO_2 hydrogenation to formate and to CO on (a) D(Ni_4) and (b) H(Ni_4). Only transition state (TS) with the highest barrier for each path is shown.

on these oxides is inevitable. In CO_2 hydrogenation over the metal catalysts supported on these oxides, CO should be the key intermediate, and methane is expected to be the dominant product [35,60–65].

Water is an unavoidable by-product in CO_2 hydrogenation. Varying the reaction conditions will change the partial pressure of water, and thereby, affect the coverage of hydroxyls. Furthermore, the intrinsic properties of the oxide support and pretreatment condition will affect the hydroxyl coverage. Based on our results, a higher coverage of surface hydroxyls on the oxide would favor the formation of the carboxyl species, which will dissociate to produce CO. Consequently, a higher coverage of surface hydroxyls will benefit the reverse WGS reaction and likely leads to methane in the final product. On the other hand, the surface hydroxyls on the oxide will significantly weaken the metal–support interaction and destabilize the catalyst. Therefore, the coverage of surface hydroxyls has to be controlled to balance the product distribution and catalyst stability.

4. Conclusions

In the present study, we analyzed the elementary steps leading to the formation of formate and CO, two possible intermediates in CO_2 hydrogenation on Ni/γ-Al_2O_3, using the DFT slab calculations. A 4-atom Ni cluster, Ni_4, was placed on the dry γ-Al_2O_3(1 1 0) surface and the hydroxylated γ-Al_2O_3(1 1 0) surface in turn to construct the model catalysts: D(Ni_4) and H(Ni_4). On D(Ni_4), the reaction energy and activation barrier with respect to the co-adsorbed CO_2 and H for formate formation are −0.23 eV and 1.25 eV, respectively, whereas those for CO formation are −0.48 eV and 2.13 eV, respectively. Consequently, formate formation is preferred kinetically while CO formation is more facile thermodynamically on D(Ni_4). On H(Ni_4), the reaction energy and activation barrier for formate formation become −0.36 eV and 2.32 eV, respectively, whereas those for CO formation are −0.67 eV and 0.69 eV, respectively. As such, CO formation becomes more favorable both kinetically and thermodynamically on H(Ni_4). At higher H adatom coverages, the corresponding preference on the fully dehydrated surface and hydroxylated surface is maintained. These results indicate that hydroxylation of γ-Al_2O_3 alters the pathway of CO_2 hydrogenation on Ni/γ-Al_2O_3. This change in reaction pathway will ultimately affect the distribution of the final products, and therefore, the selectivity of the reaction. The analyses may be applied to other heterogeneous catalytic reactions and help to select support according to the reaction environment.

Acknowledgments

We gratefully acknowledge supports from the Petroleum Research Fund (PRF-G44103-G10), Illinois Clean Coal Institute and the National Natural Science Foundation of China (under Contract 20990223).

Appendix A. Supplementary material

Supplementary data associated with this article can be found, in the online version, at doi:10.1016/j.jcat.2010.04.003.

References

[1] A. Dey, Y.I. Jiang, P.O. de Montellano, K.O. Hodgson, B. Hedman, E.I. Solomon, J. Am. Chem. Soc. 131 (2009) 7869–7878.
[2] S.P. de Visser, L.S. Tan, J. Am. Chem. Soc. 130 (2008) 12961–12974.
[3] M. Digne, P. Raybaud, P. Sautet, D. Guillaume, H. Toulhoat, J. Am. Chem. Soc. 130 (2008) 11030–11039.
[4] X.D. Xu, P. Servati, Nano Lett. 9 (2009) 1999–2004.
[5] Z.L. Hong, L.F. Cheng, L.T. Zhang, Y.G. Wang, J. Am. Ceram. Soc. 92 (2009) 193–196.
[6] A. Arranz, C. Palacio, D. Garcia-Fresnadillo, G. Orellana, A. Navarro, E. Munoz, Langmuir 24 (2008) 8667–8671.
[7] A.V. Bandura, J.D. Kubicki, J.O. Sofo, J. Phys. Chem. B 112 (2008) 11616–11624.
[8] Y.X. Pan, C.-j. Liu, Q. Ge, Langmuir 24 (2008) 12410–12419.
[9] M. Digne, P. Sautet, P. Raybaud, P. Euzen, H. Toulhoat, J. Catal. 226 (2004) 54–68.
[10] V.A. Tikhomirov, K. Jug, J. Phys. Chem. B 104 (2000) 7619–7622.
[11] M. Odelius, Phys. Rev. Lett. 82 (1999) 3919–3922.
[12] L. Giordano, J. Goniakowski, J. Suzanne, Phys. Rev. Lett. 81 (1998) 1271–1273.
[13] J.A. Rodriguez, J. Evans, J. Graciani, J.-B. Park, P. Liu, J. Hrbek, J.F. Sanz, J. Phys. Chem. C 113 (2009) 7364–7370.
[14] Z.P. Qu, W.X. Huang, S.T. Zhou, H. Zheng, X.M. Liu, M.J. Cheng, X.H. Bao, J. Catal. 234 (2005) 33–36.
[15] M. Daturi, L.G. Appel, J. Catal. 209 (2002) 427–432.
[16] D. Lomot, Z. Karpinski, Catal. Lett. 69 (2000) 133–138.
[17] C.J. Bertole, C.A. Mims, G. Kiss, J. Catal. 210 (2002) 84–96.
[18] F.G. Botes, Catal. Rev. 50 (2008) 471–491.
[19] S. Solomon, D. Qin, M. Manning, Z. Chen, M. Marquis, K.B. Averyt, M. Tignor, H.L. Miller (Climate Change 2007: The Physical Science Basis - Contribution of Working Group I to the Fourth Assessment Report of the Intergovernmental Panel on Climate Change), Cambridge University Press, Cambridge, UK, 2007.
[20] H. Arakawa, M. Aresta, J.N. Armor, M.A. Barteau, E.J. Beckman, A.T. Bell, J.E. Bercaw, C. Creutz, E. Dinjus, D.A. Dixon, K. Domen, D.L. DuBois, J. Eckert, E. Fujita, D.H. Gibson, W.A. Goddard, D.W. Goodman, J. Keller, G.J. Kubas, H.H. Kung, J.E. Lyons, L.E. Manzer, T.J. Marks, K. Morokuma, K.M. Nicholas, R. Periana, L. Que, J. Rostrup-Nielson, W.M.H. Sachtler, L.D. Schmidt, A. Sen, G.A. Somorjai, P.C. Stair, B.R. Stults, W. Tumas, Chem. Rev. 101 (2001) 953–996.
[21] E.E. Benson, C.P. Kubiak, A.J. Sathrum, J.M. Smieja, Chem. Soc. Rev. 38 (2009) 89–99.
[22] C.S. Song, Catal. Today 115 (2006) 2–32.
[23] A. Urakawa, F. Jutz, G. Laurenczy, A. Baiker, Chem.-Eur. J. 13 (2007) 3886–3899.
[24] E. Novak, K. Fodor, T. Szailer, A. Oszko, A. Erdohelyi, Top. Catal. 20 (2002) 107–117.
[25] S.E. Collins, M.A. Baltanas, A.L. Bonivardi, J. Catal. 226 (2004) 410–421.
[26] J.L. Falconer, E.A. Zagli, J. Catal. 62 (1980) 280–285.
[27] G.D. Weatherbee, C.H. Bartholomew, J. Catal. 77 (1982) 460–472.
[28] A. Tahri, A. Amariglio, M. Zyad, H. Amariglio, J. Chim. Phys. 90 (1993) 109–121.
[29] A. Tahri, A. Amariglio, M. Zyad, H. Amariglio, J. Chim. Phys. 90 (1993) 123–137.
[30] N.M. Gupta, V.S. Kamble, V.B. Kartha, R.M. Iyer, K.R. Thampi, M. Gratzel, J. Catal. 146 (1994) 173–184.
[31] K.D. Jung, A.T. Bell, J. Catal. 193 (2000) 207–223.
[32] S. Fujita, M. Usui, H. Ito, N. Takezawa, J. Catal. 157 (1995) 403–413.
[33] D.B. Clarke, A.T. Bell, J. Catal. 154 (1995) 314–328.
[34] F. Hutschka, A. Dedieu, M. Eichberger, R. Fornika, W. Leitner, J. Am. Chem. Soc. 119 (1997) 4432–4443.
[35] A.E. Aksoylu, A.N. Akin, Z.I. Onsan, D.L. Trimm, Appl. Catal. A – Gen. 145 (1996) 185–193.
[36] C. Schild, A. Wokaun, R.A. Koeppel, A. Baiker, J. Phys. Chem.-Us 95 (1991) 6341–6346.
[37] S. Fujita, H. Terunuma, M. Nakamura, N. Takezawa, Ind. Eng. Chem. Res. 30 (1991) 1146–1151.
[38] L.E. Cratty Jr., W.W. Russell, J. Am. Chem. Soc. 80 (1958) 767–773.
[39] D.E. Peebles, D.W. Goodman, J. Phys. Chem. 87 (1983) 4378–4387.
[40] T. Van Herwijnen, H. Van-Doesburg, A.W. De Jong, J. Catal. 28 (1973) 391–402.
[41] G. Kresse, J. Hafner, Phys. Rev. B 48 (1993) 13115–13118.
[42] G. Kresse, J. Furthmuller, Phys. Rev. B 54 (1996) 11169–11186.
[43] P.E. Blochl, Phys. Rev. B 50 (1994) 17953–17979.
[44] G. Kresse, D. Joubert, Phys. Rev. B 59 (1999) 1758–1775.
[45] J.P. Perdew, K. Burke, M. Ernzerhof, Phys. Rev. Lett. 77 (1996) 3865–3868.
[46] H.J. Monkhorst, J.D. Pack, Phys. Rev. B 13 (1976) 5188–5192.
[47] G. Henkelman, B.P. Uberuaga, H. Jonsson, J. Chem. Phys. 113 (2000) 9901–9904.
[48] G.L. Arvizu, P. Calaminici, J. Chem. Phys. 126 (2007) 194102.
[49] G.A. Cisneros, M. Castro, D.R. Salahub, Int. J. Quantum Chem. 75 (1999) 847–861.
[50] L. Giordano, G. Pacchioni, A.M. Ferrari, F. Illas, N. Rösch, Surf. Sci. 473 (2001) 213–226.
[51] G.W. Watson, R.P.K. Wells, D.J. Willock, G.J. Hutchings, J. Phys. Chem. B 105 (2001) 4889–4894.
[52] A. Yamakata, J. Kubota, J.N. Kondo, C. Hirose, K. Domen, F. Wakabayashi, J. Phys. Chem. B 101 (1997) 5177–5181.
[53] S. Katano, Y. Kim, Y. Kagata, M. Kawai, Chem. Phys. Lett. 427 (2006) 379–382.
[54] A.A. Gokhale, J.A. Dumesic, M. Mavrikakis, J. Am. Chem. Soc. 130 (2008) 1402–1414.
[55] E. Vesselli, L. De Rogatis, X.L. Ding, A. Baraldi, L. Savio, L. Vattuone, M. Rocca, P. Fornasiero, M. Peressi, A. Baldereschi, R. Rosei, G. Comelli, J. Am. Chem. Soc. 130 (2008) 11417–11422.
[56] Y. Uemura, T. Taniike, M. Tada, Y. Morikawa, Y. Iwasawa, J. Phys. Chem. C 111 (2007) 16379–16386.
[57] M. Bowker, R.A. Hadden, H. Houghton, J.N.K. Hyland, K.C. Waugh, J. Catal. 109 (1988) 263–273.
[58] A. Kiennemann, H. Idriss, J.P. Hindermann, J.C. Lavalley, A. Vallet, P. Chaumette, P. Courty, Appl. Catal. 59 (1990) 165–184.

[59] A. Wander, N.M. Harrison, J. Chem. Phys. 115 (2001) 2312–2316.
[60] X.M. Liu, G.Q. Lu, Z.F. Yan, J. Beltramini, Ind. Eng. Chem. Res. 42 (2003) 6518–6530.
[61] T. Nakayama, N. Ichikuni, S. Sato, F. Nozaki, Appl. Catal. A 158 (1997) 185–199.
[62] S. Fujita, M. Nakamura, T. Doi, N. Takezawa, Appl. Catal. A 104 (1993) 87–100.
[63] T. Suzuki, K. Saeki, Y. Mayama, T. Hirai, S. Hayashi, React. Kinet. Catal. L 44 (1991) 489–497.
[64] F. Solymosi, A. Erdohelyi, M. Lancz, J. Catal. 95 (1985) 567–577.
[65] A. Erdohelyi, M. Pasztor, F. Solymosi, Catalytic-hydrogenation of Co2 over supported palladium, J. Catal. 98 (1986) 166–177.